ISSN 1392–1207. MECHANIKA. 2023 Volume 29(1): 51–58

Passivity-Based Adaptive Robust Super-Twisting Nonlinear Control for Electro-Hydraulic System with Uncertainties and Disturbances

Haohao DU*, Chenghu JING, Bingsheng YAN***, Chunbo LIU******
**School of Mechanical and Electronic Engineering, Henan University of Technology, Zhengzhou 450001, China*
***School of Mechanical and Electronic Engineering, Henan University of Technology, Zhengzhou 450001, China*
E-mail: chjinghit@yeah.net (Corresponding author)
****School of Mechanical and Electronic Engineering, Henan University of Technology, Zhengzhou 450001, China*
*****School of Mechanical and Electronic Engineering, Henan University of Technology, Zhengzhou 450001, China*
crossref *http://dx.doi.org/10.5755/j02.mech.32405*

1. Introduction

Electro-hydraulic load simulator (EHLS) is a kind of hardware-in-the-loop equipment an important equipment, which is employed to replicate the complex load characteristics, so as to detect technical performance of the rocket servo mechanism [1-3]. Therefore, it is of great significance to develop the electrohydraulic load simulator with high precision and quick response in order to further improve the dynamic performance of rocket servo mechanism However, EHLS is subjected to motion disturbance from the tested actuator system [4-6]. Great attentions have been paid for improving performance of EHLS under actuator's motion disturbance [7-10]. However, the problem of actuator's motion disturbance has not been well solved. In the works [11, 12], a kind of electro-hydraulic load simulator was developed. It makes use of friction to reproduce torque such that the load simulator and the tested actuator system are decoupled. With the development of industry, the performance requirements of the novel EHLS are more and more high. Therefore, advanced control algorithms are shown to be a necessity for the novel EHLS. In [11], an adaptive state observer based adaptive backstepping-flatness control was proposed for torque tracking of the novel EHLS. In [12], an adaptive extended state observer-based flatness nonlinear control was developed for torque tracking of the novel EHLS. However, the uncertainties of system parameters are not considered in these works.

The backstepping method is an effective approach to ensure stability and performance in a global sense for controller design of nonlinear systems. It is widely applied to electro-hydraulic servo systems [13-16]. Backstepping design process is complex and the computation is large. Passive theory that uses passivation to achieve the control objective is also an effective method to ensure stability and performance in a global sense for controller design of nonlinear systems [17]. Compared with backstepping approach, passive-based controller is more simple and intuitive [18]. This technique has been successfully applied to a nonlinear electro-hydraulic systems and was shown to be very effective [19,20].

Certainty equivalence adaptive law was always introduced to backstepping controllers through Lyapunov functions to account for parametric uncertainties [21-23]. But, the certainty equivalence adaptive approaches only estimate constant or slow time-varying parameters and disturbances. Sliding mode control (SMC) is one of the most promising robust control techniques to reject time-varying disturbances and uncertainties [24, 25]. To handle parameter uncertainties and disturbances, adaptive backstepping sliding mode controller [26] were proposed for electro-hydraulic systems. But chattering is caused by sliding mode controller, which can degrade the closed-loop system performance [27, 28]. Higher order SMC has been emerged that alleviates chattering. Super twisting algorithm (STA) has been proved to be effective HOSM approach for relative degree one system [29, 30]. However, it only applies to relative degree one system for alleviating chattering.

Motivated by the above discussions, a passive-based adaptive robust super-twisting nonlinear controller is proposed by combining passive approach, adaptive law and super-twisting control to improve the torque tracking of the novel EHLS. The proposed control strategy was designed by recursive design approach. Passivity theory and Lyapunov function guarantee the stability of this electro-hydraulic control system. In the process of controller design, the adaptive algorithm and super-twisting control are respectively designed in the two subsystem to solve the corresponding uncertainties and disturbances.

2. Dynamic models and problem formulation

In general, the load torque for actuator testing can be generated by the deformation of elastic connecting shaft, which is determined by the position between the load actuator and tested actuator. So the tested actuator' motion is the key problem to achieve good loading torque tracking for conventional EHLS. Friction torque may be generated through relative rotation of two objects in contact with each other. And friction torque may be used to simulate load torque. The novel EHLS shown in Fig. 1 is developed. The basic components in the electro-hydraulic friction load simulator are hydraulic cylinders, hydraulic power, servo valve, friction plates, torque sensor, hydraulic swing motor and electric motor.

The friction disk A2 and B2 can rotate along with the shaft and move along the shaft. The electric motor needs to keep rotating all the time when the actuator is tested. To obtain bidirectional motion, the gear set is used to generate rotation in different directions. So the friction disk A1 and B1 are respectively rotating by gear set transmission. To generate friction, Friction disk A1 and A2, Friction disk B1 and B2 must keep rotating relatively all the time. The bidirectional friction torque that results from rotary friction pairs acts on the shaft of tested actuator to simulate load. The pressure on the friction plate can be adjusted by valve-controlled hydraulic cylinders, so as to regulate loading torque. Then the actual loading torque from torque sensor is fed back to controller to achieve the torque servo control. The control goal is to make the friction torque track any specified reference torque as closely as possible by adjusting the output pressure of hydraulic cylinder.

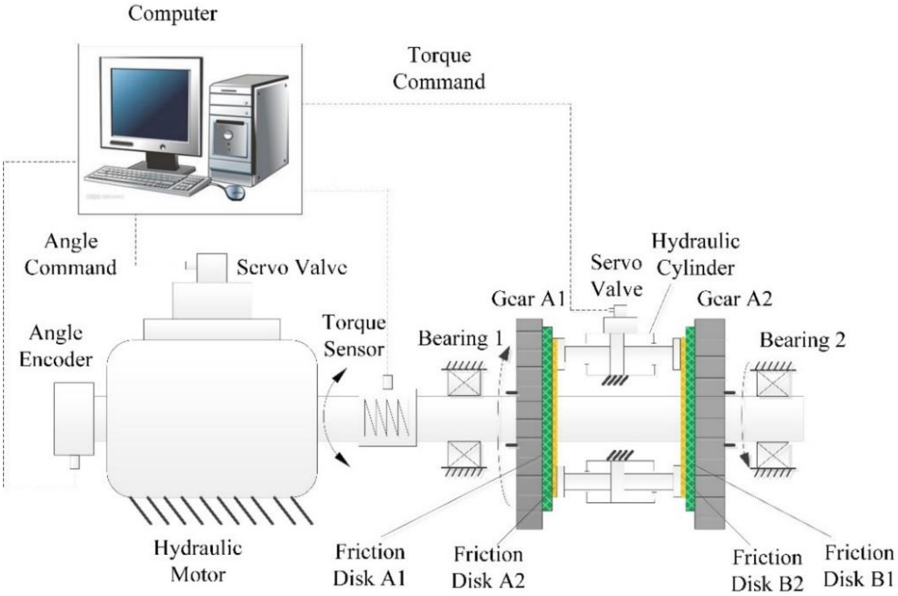

Fig. 1 Schematic diagram of the electro-hydraulic loading system

In the novel EHLS, friction torque is used to simulate aerodynamic load acting on the actuator system of aircraft. The friction torque is generated by rotary friction pairs. Using the theory of calculus, friction torque on the contact surface can be expressed as:

$$T = \int_{R_1}^{R_2} r \cdot \mu p 2\pi dr = \mu RF, \tag{1}$$

where: $R = \dfrac{2}{3}\dfrac{R_2^3 - R_1^3}{R_2^2 - R_1^2}$ denotes equivalent friction radius, m; R_1 is the internal radius of frictional contact area, m; R_2 is the external radius of frictional contact area, m; μ is the friction coefficient; F is the force acting on a pair of friction pairs, N.

Pressing force of friction pairs is given by:

$$F = Ky, \tag{2}$$

where: K is the load stiffness, N/m; y is the piston position of the hydraulic cylinder, m.

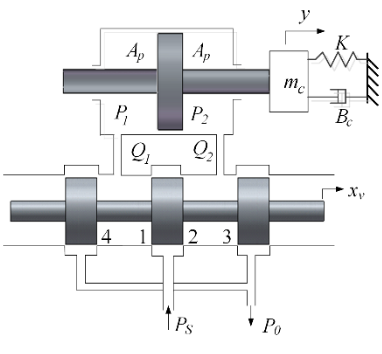

Fig. 2 Oil circuit of valve-controlled hydraulic

The valve-controlled hydraulic cylinder shown in Fig. 2 is crucial element in this system. In Fig. 2 A_p is the effective pressure area of the piston, m^2; P_s is oil supply pressure, Pa; $P_0 \approx 0$ is return oil pressure, Pa; P_1 is pressure of left chamber, Pa; P_2 is pressure of right chamber, Pa; Q_1 is flow rate of left chamber, m^3/s; Q_2 is flow rate of right chamber, m^3/s; m_c is the equivalent mass of load, kg; B_c is the viscous damping coefficient of the pistons, N/(m/s); x_v is the spool position of the servo-valve, m; 1, 2, 3 and 4 respectively represent the ID of the orifices composed of valve core and valve body The basic set of equations describing the dynamics of a valve-controlled hydraulic motor contains the following equations.

The control flow equation of the hydraulic valve for the load flow rate is written as

$$Q_L = C_d w x_v \sqrt{\frac{1}{\rho}(P_s - \mathrm{sign}(x_v) P_L)}, \tag{3}$$

where: Q_L is load flow rate, m^3/s; C_d is discharge coefficient of servo valve; w represents valve spool area gradient, m; ρ is the fluid density, kg/m^3; P_L is load pressure, Pa.

By applying the continuity law to each chamber of the hydraulic cylinder, the load flow rate continuity equation is given by:

$$Q_L = A_p \dot{y} + C_{ct} P_L + \frac{V_t}{4\beta_e}\dot{P}_L, \tag{4}$$

where: $C_{ct}=C_{ip} + C_{ep}/2$ is the total leakage coefficient, m^5/(Nm); C_{ip} is the internal leakage coefficient, m^5/(Nm); C_{ep} is the external leakage coefficient, m^5/(Nm); y is the piston position of the hydraulic cylinder, m; V_t is the total equivalent control volume, m^3; β_e is the effective volume elasticity modulus of the hydraulic fluid, N/m^2.

The friction disks are driven by the hydraulic cylinder to press down with each other. By applying Newton's second law, the load dynamics is described by:

$$A_p P_L = m_c \ddot{y} + B_c \dot{y} + Ky + f_d, \tag{5}$$

where: f_d is the friction.

In general, the dynamic response of the electrical components in the system is much larger than the dynamic response of the mechanical or hydraulic components. The relationship between spool displacement of servo valve and input voltage is approximately linear:

$$x_v = k_v u, \tag{6}$$

where: u is the input current of the torque motor, V; k_u is the gain, m/V.

Combining Eqs. (1)-(6) and choose state variable as $x_1 = T, x_2 = \dot{T}, x_3 = P_L$ the state-space form of the electro-hydraulic friction loading system mentioned above can be described as:

$$\begin{cases} \dot{x}_1 = x_2 \\ \dot{x}_2 = \dfrac{1}{m_c}\left(-Kx_1 - B_c x_2\right) + \dfrac{\mu RKA_p}{m_c} x_3 - \dfrac{\mu RKA_p}{m_c} f_d \\ \dot{x}_3 = \dfrac{4\beta_e}{V_t}\left(-\dfrac{A}{\mu RK} x_2 - C_t x_3\right) + g\left(x_3, u\right)u + f_x \end{cases}, \tag{7}$$

where: f_x represents the unmodeled dynamics, $g\left(x_3, u\right) = \dfrac{4\beta_e C_d w k_v}{V_t\sqrt{\rho}}\sqrt{(P_s - \text{sign}(u)x_3)}$.

Define parameters: $\theta_1 = \dfrac{K}{m_c}, \theta_2 = \dfrac{B_c}{m_c}, \Delta_1 = \dfrac{\mu RKA_p}{m_c} f_d, \theta_3 = \dfrac{\mu RKA_p}{m_c}$, $f\left(x_2, x_3\right) = -\dfrac{4\beta_e}{V_t}\left(\dfrac{A_p}{\mu RK} x_2 + C_t x_3\right)$. The system is subjected to parametric uncertainties due to the variations of m_c, K, B_c, μ, f, β_e, V_t, C_t and ρ. So these defined parameters are uncertain and slowly-varying. Define $f_0\left(x_2, x_3\right)$ and $g_0\left(x_3, u\right)$ are nominal values of $f\left(x_2, x_3\right)$ and $g\left(x_3, u\right)$, respectively. The parameter deviations and unmodeled dynamics f_x are lumped to matched disturbance term $\Delta_2 = \Delta f\left(x_2, x_3\right) + \Delta g\left(x_3, u\right)u + f_x$. According to the above definitions, the system (7) is rewritten as:

$$\begin{cases} \dot{x}_1 = x_2 \\ \dot{x}_2 = -\theta_1 x_1 - \theta_2 x_2 + \theta_3 x_3 + \Delta_1 \\ \dot{x}_3 = f_0\left(x_2, x_3\right) + g_0\left(u, x_3\right)u + \Delta_2 \end{cases}, \tag{8}$$

Assumption Δ_1 and Δ_2 are unknown but bounded. $\left\|\Delta_1\right\| \le \rho_1$, $\left\|\dot{\Delta}_1\right\| \approx 0$, $\left\|\Delta_2\right\| \le \rho_2$, $\left\|\dot{\Delta}_2\right\| \le \beta$, ρ_1, ρ_2, γ are positive.

In order to implement the controller design, we regard each formula in system (8) as a subsystem. So this system consists of three subsystems.

3. Controller design

Define $x^d = \begin{bmatrix} x_1^d & x_2^d & x_3^d \end{bmatrix}$ as the desired state vector. So, the state tracking errors are written as:

$$e_i = x_i - x_i^d \quad i = 1, 2, 3. \tag{9}$$

Differentiate each tracking error to create the tracking error dynamics as follows:

$$\begin{aligned} \dot{e}_1 &= \dot{x}_1 - \dot{x}_1^d = x_2 - \dot{x}_1^d \\ \dot{e}_2 &= \dot{x}_2 - \dot{x}_2^d = -\theta_1 x_1 - \theta_2 x_2 + \theta_3 x_3 + \Delta_1 - \dot{x}_2^d \\ \dot{e}_3 &= \dot{x}_3 - \dot{x}_3^d = f_0\left(x_2, x_3\right) + g_0\left(u, x_3\right)u + \Delta_2 - \dot{x}_3^d \end{aligned}. \tag{10}$$

The quadratic Lyapunov functions for three subsystems are chosen as:

$$V_i = \frac{1}{2} e_i^2 \quad i = 1, 2, 3. \tag{11}$$

Given an arbitrary desired torque x_1^d, the virtual control inputs x_2^d, x_3^d and the actual control input u are designed as:

$$\begin{aligned} x_2^d &= \dot{x}_1^d - k_1 e_1 \\ x_3^d &= \frac{1}{\theta_3}\left(\theta_1 x_1 + \theta_2 x_2 + \dot{x}_2^d - \Delta_1 - k_2 e_2\right) \\ u &= \frac{1}{g_0\left(u, x_3\right)}\left(-f_0\left(x_2, x_3\right) + \dot{x}_3^d - \Delta_2 - k_3 e_3\right) \end{aligned}, \tag{12}$$

Substituting Eq. (12) into Eq. (10), a chain of interconnected tracking error dynamics can be derived:

$$\begin{aligned} \dot{e}_1 &= -k_1 e_1 + e_2 \\ \dot{e}_2 &= -k_2 e_2 + g_{20} e_3 \\ \dot{e}_3 &= -k_3 e_3 \end{aligned}. \tag{13}$$

Based on the Eq. (13), its time derivative along Eq. (11) is given as:

$$\begin{aligned} \dot{V}_1 &= -k_1 e_1^2 + e_1 e_2 \\ \dot{V}_2 &= -k_2 e_2^2 + g_{20} e_2 e_3 \\ \dot{V}_3 &= -k_3 e_3^2 \end{aligned}, \tag{14}$$

The first two equations of Eq. (13) is rewritten by:

$$\begin{aligned} \underset{input}{e_2}\ \underset{output}{e_1} &= \dot{V}_1 + k_1 e_1^2 \\ \underset{input}{g_{20} e_3}\ \underset{output}{e_2} &= \dot{V}_2 + k_2 e_2^2 \end{aligned}. \tag{15}$$

Then Eq. (14) shows that the relationship between e_i and e_{i+1} is strictly output passive [34] and $\dot{e}_i = -k_i e_i \quad \forall \mathrm{i} \in \{1, 2\}$ is zero-state observable. Therefore, each subsystem is bounded input bounded output (BIBO) stable. Serial interconnections of BIBO stable system are also BIBO stable. Further, the 3th tracking error dynamics becomes:

$$\dot{e}_3 = -k_3 e_3. \tag{16}$$

We apply Barbalat's Lemma (Khalil, 1996) to conclude that e_3 converges exponentially to zero at the convergence rate k_3. Then e_1 and e_2 converges to zero.

Based on the passive characteristics of the system, the theoretical controller is obtained. But parametric uncertainties, disturbances and unmodeled dynamics may deteriorate the performance of passive controller. In this paper, parameter adaptive method is adopted in the second subsystem to solve the problem of parameter uncertainty.

Define parameter error $\tilde{\theta}_i = \theta_i - \hat{\theta}_i$, a Lyapunov function for the second subsystem is considered:

$$V_2' = \frac{1}{2}e_2^2 + \frac{1}{2}\sum_{i=1}^{3}\frac{1}{\alpha_i}\tilde{\theta}_i^2 + \frac{1}{2r}\tilde{\Delta}_1^2. \quad (17)$$

Its time derivative along Eq. (11) is given as:

$$\begin{aligned}\dot{V}_2' &= e_2\dot{e}_2 + \sum_{i=1}^{3}\frac{1}{\alpha_i}\tilde{\theta}_i\dot{\tilde{\theta}}_i + \frac{1}{r}\tilde{\Delta}_1\dot{\tilde{\Delta}}_1 = e_2\left(-\theta_1 x_1 - \theta_2 x_2 + \theta_3 x_3 + \Delta_1 - \dot{x}_2^d\right) + \sum_{i=1}^{3}\frac{1}{\alpha_i}\tilde{\theta}_i\dot{\tilde{\theta}}_i + \frac{1}{r}\tilde{\Delta}_1\dot{\tilde{\Delta}}_1 = \\ &= e_2\left(-\tilde{\theta}_1 x_1 - \tilde{\theta}_2 x_2 + \tilde{\theta}_3 x_3 + \hat{\theta}_3 e_3 + \tilde{\Delta}_1 - k_2 e_2\right) + \sum_{i=1}^{3}\frac{1}{\alpha_i}\tilde{\theta}_i\dot{\tilde{\theta}}_i + \frac{1}{r}\tilde{\Delta}_1\dot{\tilde{\Delta}}_1.\end{aligned} \quad (18)$$

The adaptive law is designed as:

$$\begin{aligned}&\dot{\hat{\theta}}_1 = -\alpha_1 x_1 e_2 \quad \dot{\hat{\theta}}_2 = -\alpha_2 x_2 e_2 \\ &\dot{\hat{\theta}}_3 = \alpha_3 x_3 e_2 \quad \dot{\hat{\Delta}}_1 = r e_2\end{aligned}. \quad (19)$$

So the virtual control input in the second subsystem is written as:

$$x_3^d = \frac{1}{\hat{\theta}_3}\left(\hat{\theta}_1 x_1 + \hat{\theta}_2 x_2 + \dot{x}_2^d - \hat{\Delta}_1 - k_2 e_2\right). \quad (20)$$

The parameters are unknown and slow time-varying so that $\dot{\theta}_i$ is approximately equal to zero. So $\dot{\hat{\theta}}_i \approx -\dot{\tilde{\theta}}_i$ is reasonable. Substituting Eq. (18) into Eq. (17), one obtains:

$$\dot{V}_2' = -k_2 e_2^2 - \hat{\theta}_3 e_2 e_3. \quad (21)$$

Super-twisting sliding mode control is used in the second subsystem to eliminate disturbances and unmodeled dynamics. Define a sliding manifold of the following form:

$$s = e_3 + k_3\int e_3 dt. \quad (22)$$

The following actual control law is proposed as:

$$u = \frac{1}{g_0(u, x_3)}\left(-f_0(x_2, x_3) + \dot{x}_3^d - k_3 e_3 - \lambda_1 |s|^{\frac{1}{2}} sgn(s) - \lambda_2\int sgn(s)dt\right), \quad (23)$$

From Eq. (21), one obtains:

$$\begin{aligned}&\dot{s} = \dot{e}_3 + k_3 e_3 = \\ &= f_0(x_2, x_3) + g_0(u, x_3)u + \Delta_2 - \dot{x}_3^d + k_3 e_3.\end{aligned} \quad (24)$$

Substituting actual control law (23) into Eq. (24), one obtains:

$$\begin{aligned}&\dot{s} = -\lambda_1|s|^{\frac{1}{2}}\operatorname{sgn}(s) - \lambda_2\int sgn(s)dt + \Delta_2 = \\ &= -\lambda_1|s|^{\frac{1}{2}}\operatorname{sgn}(s) - \lambda_2\int sgn(s)dt + \Delta_2.\end{aligned} \quad (25)$$

Eq. (25) is rewritten as:

$$\begin{aligned}&\dot{s} = -\lambda_1|s|^{\frac{1}{2}} sgn(s) + \sigma \\ &\dot{\sigma} = -\lambda_2 sgn(s) + \dot{\Delta}_2\end{aligned}. \quad (26)$$

Choose the Lyapunov function for the third subsystem:

$$V_3' = 2\lambda_2|s| + \frac{1}{2}\sigma^2 + \frac{1}{2}\left(\lambda_1|s|^{1/2} sgn(s) - \sigma\right)^2. \quad (27)$$

Choose the vector $\zeta = \left[|s|^{1/2}\operatorname{sgn}(s) \quad \sigma\right]^T$, and the Lyapunov function V_3' can be rewritten as:

$$V_3' = \zeta^T P\zeta, , \quad (28)$$

where: $P = \begin{bmatrix} 2\lambda_2 + \frac{1}{2}\lambda_1^2 & -\frac{1}{2}\lambda_1 \\ -\frac{1}{2}\lambda_1 & 1\end{bmatrix}$.

Its time derivative along the vector ζ as follows:

$$\dot{\zeta} = \frac{1}{|s|^{1/2}}\left(A\zeta + B\tilde{\delta}\right), \quad (29)$$

where: $A = \begin{bmatrix} -\frac{1}{2}\lambda_1 & \frac{1}{2} \\ -\lambda_2 & 0\end{bmatrix}$, $B = \begin{bmatrix}0 \\ 1\end{bmatrix}$, $\tilde{\delta} = |s|^{1/2}\dot{\Delta}_2$.

The transformed perturbation $\tilde{\delta} = |s|^{1/2}\dot{\Delta}_2 \le \beta|s|^{1/2}$. As a consequence, $\omega(\tilde{\delta}, \zeta) = -\tilde{\delta}^2 + \beta^2|s| \ge 0$. The derivative of the candidate Lyapunov function along the states of the system (26) is given as the following actual control law is proposed as:

$$\dot{V}_3' = \frac{1}{|s|^{1/2}}\left[\zeta^T\left(A^TP + PA\right)\zeta + \tilde{\delta}^T B^T P\zeta + \zeta^T PB\tilde{\delta}\right] = \frac{1}{|s|^{1/2}}\begin{bmatrix}\zeta\\ \tilde{\delta}\end{bmatrix}^T \begin{bmatrix}A^TP+PA & PB\\ B^TP & 0\end{bmatrix}\begin{bmatrix}\zeta\\ \tilde{\delta}\end{bmatrix} \le$$
$$\le \frac{1}{|s|^{1/2}}\left\{\begin{bmatrix}\zeta\\ \tilde{\delta}\end{bmatrix}^T \begin{bmatrix}A^TP+PA & PB\\ B^TP & 0\end{bmatrix}\begin{bmatrix}\zeta\\ \tilde{\delta}\end{bmatrix} + \omega\left(\tilde{\delta},\zeta\right)\right\} \le \frac{1}{|s|^{1/2}}\begin{bmatrix}\zeta\\ \tilde{\delta}\end{bmatrix}^T \begin{bmatrix}A^TP+PA+\beta^2C^TC & PB\\ B^TP & -1\end{bmatrix}\begin{bmatrix}\zeta\\ \tilde{\delta}\end{bmatrix} \le$$
$$\le \frac{1}{|s|^{1/2}}\begin{bmatrix}\zeta\\ \tilde{\delta}\end{bmatrix}^T \begin{bmatrix}A^TP+PA+\varepsilon P+\beta^2C^TC-\varepsilon P & PB\\ B^TP & -1\end{bmatrix}\begin{bmatrix}\zeta\\ \tilde{\delta}\end{bmatrix}. \tag{30}$$

The robust stability analysis can be performed through the LMI. Suppose that there exist a symmetric and positive definite matrix $P = P^T > 0$ and $\varepsilon > 0$ so that the following algebraic LMI equation is satisfied, then $\dot{V}_3' \le -\frac{1}{|s|^{1/2}}\varepsilon\zeta^T P\zeta$.

$$\begin{bmatrix}A^TP+PA+\varepsilon P+\beta^2C^TC & PB\\ B^TP & -1\end{bmatrix} \le 0. \tag{31}$$

In this case all vectors of system (26) converge to the origin in finite time for all perturbations satisfying $\omega\left(\tilde{\delta},\zeta\right) \ge 0$.

According to the classical circle criterium [9], the algebraic LMI (30) will be satisfied if and only if the Nyquist diagram of the transfer function $G(s) = C(sI-A)^{-1}B$ is contained in the circle centered in the origin and with radius β, that is, if:

$$\max_{\omega}\left|G(j\omega)\right| < \frac{1}{\beta}, \tag{32}$$

note that,

$$G(s) = \frac{1}{2s^2 + \lambda_1 s + \lambda_2}. \tag{33}$$

According to the derivative $\frac{d}{d\omega}\left|G(j\omega)\right|^2$ and the second derivative $\frac{d^2}{d\omega^2}\left|G(j\omega)\right|^2$ along the transfer function $G(s)$, it can be deduced that:

$$\max_{\omega}\left|G(j\omega)\right|^2 = \begin{cases}\dfrac{1}{\lambda_2^2} & \text{if}\lambda_1^2 > 4\lambda_2\\[2ex] \dfrac{1}{\lambda_1^2\left(\lambda_2 - \dfrac{3}{16}\lambda_1^2\right)} & \text{if}\lambda_1^2 \le 4\lambda_2\end{cases}. \tag{34}$$

There are two possibilities of selecting the gains $\lambda_1 > 0$, $\lambda_2 > 0$ so that the STA will converge to the origin in finite time, despite of a perturbation bounded by β: 1) Select λ_2 such that $\lambda_2 > \beta$ and then select $\lambda_1^2 > 4\lambda_2$; 2) Select $\lambda_1 > 0$ and $\lambda_2 > 0$ such that both inequalities $\lambda_1^2\left(\lambda_2 - \frac{3}{16}\lambda_1^2\right) > \beta^2$ and $\lambda_1^2 > 4\lambda_2$ are satisfied.

By choosing one of two possibilities on the gains, in this paper we can then deduce conditions on gains λ_1 and λ_2 as follows:

$$\begin{matrix}\lambda_2 > \beta\\ \lambda_1^2 > 4\lambda_2\end{matrix}. \tag{35}$$

Eq. (30) is written as:

$$\dot{V}_3' \le -\frac{1}{|s|^{1/2}}\varepsilon\zeta^T P\zeta = -\frac{\varepsilon}{|s|^{1/2}}V_3'. \tag{36}$$

Moreover, this Lyapunov function is positive definite and the standard quadratic forms. Recall the standard inequality for quadratic forms:

$$\lambda_{min}\{P\}\|\zeta\|_2^2 \le V_3' \le \lambda_{max}\{P\}\|\zeta\|_2^2, \tag{37}$$

note that,

$$|s|^{1/2} \le \|\zeta\|_2 \le \frac{V_3^{1/2}}{\lambda_{\min}^{1/2}\{P\}}. \tag{38}$$

Eq. (36) is rewritten in this form:

$$\dot{V}_3' \le -\tau V_3', \tag{39}$$

where: $\tau = \varepsilon\lambda_{min}^{1/2}\{P\}$.

Eq. (39) shows that V_3' is a strong Lyapunov function and that the trajectories [s, σ] converge to the zero in finite time. So $e_3 = 0$ and $\dot{e}_3 = 0$ is reached in finite time. According to the passive property of the system, it can be obtained that e_1 and e_2 also converge to the zero in finite time.

4. Simulation and discussion

To investigate the performance of the proposed method, simulations are implemented. The sampling interval was set as 0.001 s.

In order to verify the performance of the proposed controller, two other controllers were chosen for a contrast. Controller simulation parameters in this paper are chosen as following:

1) PBARSNC: A passive-based adaptive robust super-twisting nonlinear controller is proposed in this paper and described above. The control gains are given as follows: $k_1 = 650$, $k_2 = 12000$, $k_3 = 10000$, $\alpha_1 = 200$, $\alpha_2 = 0.1$, $\alpha_3 =$

$= 1\times10^{-6}$, $r = 1\times10^5$, $\lambda_1 = 4\times10^5$, $\lambda_2 = 1\times10^3$.

2) PBC: The passive-based controller was described in this paper. Different from the proposed controller, this passive-based controller has no parameter adaptive and robust compensation control. The control gains are the same as the parameters of the proposed controller.

3) PID: This is the traditional proportional—integral–derivative controller. And its gains tuned carefully via an error-and-try method are $k_p = 1.8$, $k_i = 3.2$ and $k_d = 0.0011$, which denote the proportional gain, integral gain and derivative gain, respectively.

To compare the performance of these three controllers, we employ sinusoidal torque command $x_1 = 30sin(2\pi\times10t)$ to test these three controllers. In reality, all the parameters in system (7) can be cannot be accurately derived. So adaptive law and robust super-twisting are used in the proposed controller. The initial value of adaptive parameters is set to $\theta_{10} = 0$, $\theta_{20} = 0$ and $\theta_{30} = 21.4$. Fig. 3 shows the tracking performance of three different controllers. Fig. 3, a gives the torque tracking of a cycle. To facilitate the contrast, Fig. 3, b gives the torque tracking error within 0-0.5 seconds. It can be seen in Fig. 3 that the tracking errors of the proposed PBARSNC, PBC and PID are in the range -1.7 N·m to 0.6 N·m, -0.4 N·m to -0.1 N·m and -2 N·m to -2 N·m respectively. In 0-0.1 s, tracking error of the proposed controller is relatively large due to the adaptive parameters convergence process.

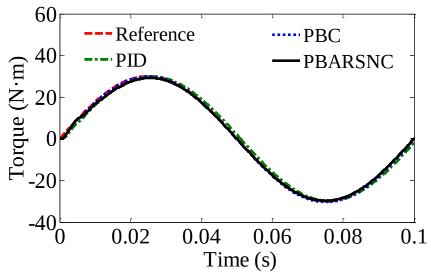

a) Torque tracking

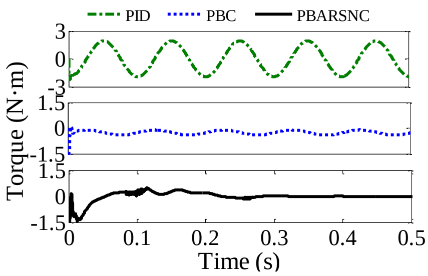

b) Tracking error of PID

Fig. 3 Tracking performance of the different controllers

Fig. 4 presents corresponding parameter convergence process. In steady state, the peak error is smallest in the three controllers, 0.01 N·m. Due to the friction and external load, tracking error of PBC have a negative offset. Compared with the others, PID controller have phase lag problem. PBARSNC and PBC can employ the system model to achieve accurate model-based, amending the phase lag problem and gets better stability.

Furthermore, the matched disturbance and low time-varying parameters variations are introduced to verify the robustness capability of the proposed controller against parametric uncertainties, disturbances and unmodeled dynamics. The mathematical model based on Simulink is set up where system parameters and disturbance are easy to be changed. In this system, the parameters β_e, μ, f_d is typical low time-varying parameters. Those parameters are set to $\beta_e = 3.5\times10^8 sin(5t) + 7\times10^8$, $\mu = 0.2+0.02sin(2t)$, $f_d = 200+100sin(5t)$. The responding tracking performance of three different controllers in this case are shown in Fig. 5. Fig. 5 shows that the proposed controller is able to achieve the best performance in the presence of parametric uncertainties and parameters variations.

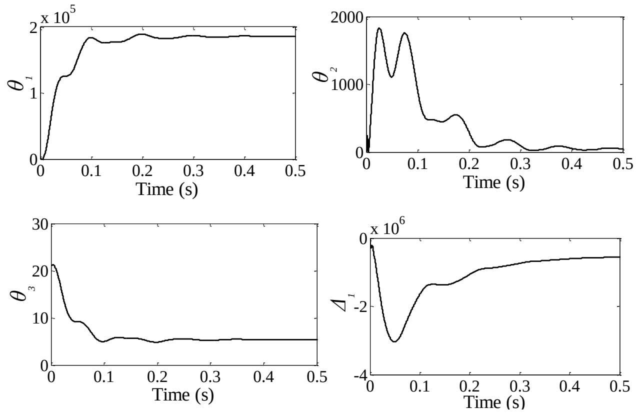

Fig. 4 Adaptive parameters convergence process

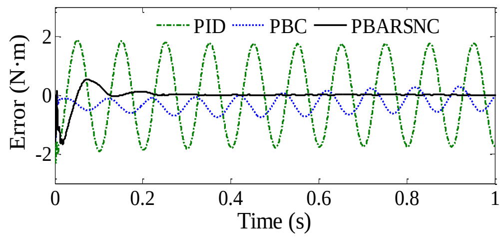

Fig. 5 Tracking error with parameters variations

Besides parameters variations, the matched disturbance $u_d = sin(85t)$ and $u_d = sin(135t)$ are introduced into system, respectively. The responding tracking error of three different controllers in the presence of parametric uncertainties, disturbances and unmodeled dynamics are shown in Fig. 6.

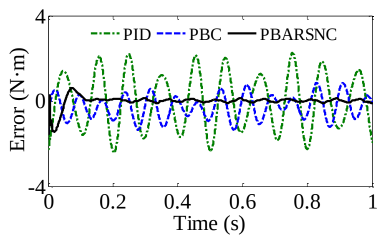

a) $u_d = \sin(85t)$

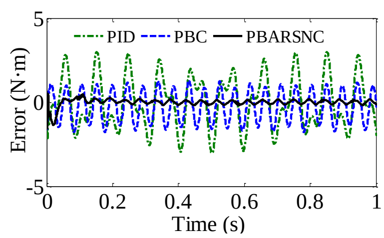

b) $u_d = 2\sin(135t)$

Fig. 6 Tracking error with input disturbances

Fig. 6, a shows that the maximum tracking errors of the proposed PBARSNC, PBC and PID are stable at 0.15 N·m, 1.2 N·m and 2.2 N·m, respectively. It can be seen in Fig. 6, b that the maximum tracking errors of the proposed PBARSNC, PBC and PID are stable at 0.3 N·m, 1.8 N·m and 3 N·m, respectively. Evidently, the performance of the three controllers becomes worse as the disturbance becomes violent. Compared to the other two controllers, the proposed controller has stronger robustness against parametric uncertainties, parameters variations and input disturbances. So it is able to achieve a better tracking performance in the presence of various types of disturbances.

5. Conclusions

In this paper, a passive-based adaptive robust super-twisting nonlinear controller (PBARSNC) has been proposed for the novel EHLS to reject disturbances and uncertainties. Passive property of the electro-hydraulic system has been adopted to design this controller. In order to achieve high accuracy torque tracking control for the novel EHLS, different types of disturbances have been considered in the design process. Considering parameter uncertainties and constant or slowly varying disturbances, adaptive law is adopted in the passivity-based controller. Furthermore, super-twisting second-order slide mode control is used to reject uncertainties and matched disturbances. The proposed control law has an exponentially convergence transient performance. Moreover, the simulation results show that the proposed passive-based adaptive robust super-twisting nonlinear control method greatly compensates the effects of matched disturbances, uncertainties and external disturbances and improves the system tracking accuracy and robustness, in comparison with traditional PID control and passive-based control. In the future work, the proposed control law will be applied to the practical electro-hydraulic system to verify the high-accuracy tracking performance.

Acknowledgments

This work was supported in part by the Foun-dation of the Education Department of Henan Province (No. 23A460006), the Foundation of Henan University of Technology (No.2021BS071), the Foundation of the Science and Technology Department of Zhengzhou (No. 22ZZRDZX 17), the Innovative Funds Plan of Henan University of Technology (No. 2020ZKCJ28) and Pre-research Project of SongShan Laboratory (No. YYJC072022020).

References

1. **Wang, C.; Jiao, Z.; Quan, L.** 2015. Adaptive velocity synchronization compound control of electro-hydraulic load simulator, Aerospace Science and Technology 42: 309-321. https://doi.org/10.1016/j.ast.2015.01.018.
2. **Nauparac, D. B.; Pršić, D. H.; Miloš, M. V.; Todić, I. S.** 2015. Different modeling technologies of hydraulic load simulator for thrust vector control actuator, Tehnički vjesnik 22(3): 599-606. https://doi.org/10.17559/tv-20140621063240.
3. **Karpenko, M.; Sepehri, N.** 2009. Hardware-in-the-loop simulator for research on fault tolerant control of electrohydraulic actuators in a flight control application, Mechatronics 19(7): 1067-1077. https://doi.org/10.1016/j.mechatronics.2009.01.008.
4. **Zhao, J.; Shen, G.; Yang, C.; Liu, G.; Yin, L.; Han, J.** 2013. Feel force control incorporating velocity feed-forward and inverse model observer for control loading system of flight simulator, Proceedings of the Institution of Mechanical Engineers, Part I: Journal of Systems and Control Engineering 227(2): 161-175. https://doi.org/10.1177/0959651812464465.
5. **Zhao, J.; Shen, G.; Yang, C.; Zhu, W.; Yao, J.** 2018. A robust force feed-forward observer for an electro-hydraulic control loading system in flight simulators, ISA transactions 89: 198-217. https://doi.org/10.1016/j.isatra.2018.12.012.
6. **Jing, C.; Xu, H.; Jiang, J.** 2019. Dynamic surface disturbance rejection control for electro-hydraulic load simulator, Mechanical Systems and Signal Processing 134: 106293. https://doi.org/10.1016/j.ymssp.2019.106293.
7. **Jacazio, G.; Balossini, G.** 2007. Real-time loading actuator control for an advanced aerospace test rig, Proceedings of the Institution of Mechanical Engineers, Part I: Journal of Systems and Control Engineering 221(2): 199-210. https://doi.org/10.1243/09596518JSCE269.
8. **Kang, S.; Nagamune, R.; Yan, H.** 2020. Almost disturbance decoupling force control for the electro-hydraulic load simulator with mechanical backlash, Mechanical Systems and Signal Processing 135: 106400. https://doi.org/10.1016/j.ymssp.2019.106400.
9. **Han, S.; Jiao, Z.; Yao, J.; Shang, Y.** 2014. Compound velocity synchronizing control strategy for electro-hydraulic load simulator and its engineering application, Journal of Dynamic Systems, Measurement, and Control 136(5): 1–13. https://doi.org/10.1115/1.4026921.
10. **Wang, C.; Jiao, Z.; Wu, S.; Shang, Y.** 2013. An experimental study of the dual-loop control of electro-hydraulic load simulator (EHLS), Chinese Journal of Aeronautics 26(6): 1586-1595. https://doi.org/10.1016/j.cja.2013.10.002.
11. **Zheng, D.; Xu, H.** 2016. Adaptive backstepping-flatness control based on an adaptive state observer for a torque tracking electrohydraulic system, IEEE/ASME Transactions on Mechatronics 21(5): 2440-2452. https://doi.org/10.1109/TMECH.2015.2513205.
12. **Jing, C.; Xu, H.; Jiang, J.** 2020. Practical torque tracking control of electro-hydraulic load simulator using singular perturbation theory, ISA transactions 102: 304-313. https://doi.org/10.1016/j.isatra.2020.02.035.
13. **Bakhshande, F.; Söffker, D.** 2018. Proportional-integral-observer-based backstepping approach for position control of a hydraulic differential cylinder system with model uncertainties and disturbances, Journal of Dynamic Systems, Measurement, and Control 140(12): 121006. https://doi.org/10.1115/1.4040662.
14. **Guo, Q.; Wang, Q.; Li, X.** 2019. Finite-time convergent control of electrohydraulic velocity servo system under uncertain parameter and external load, IEEE Transactions on Industrial Electronics 66(6): 4513-4523.

https://doi.org/10.1109/TIE.2018.2860533.
15. **Ba, D. X.; Ahn, K. K.; Truong, D. Q.; Park, H. G.** 2016. Integrated model-based backstepping control for an electro-hydraulic system, International Journal of Precision Engineering and Manufacturing 17(5): 565-577.
https://doi.org/10.1007/s12541-016-0069-x.
16. **Yao, J.; Jiao, Z.; Ma, D.** 2014. Extended-state-observer-based output feedback nonlinear robust control of hydraulic systems with backstepping, IEEE Transactions on Industrial Electronics 61(11): 6285-6293.
https://doi.org/10.1109/TIE.2014.2304912.
17. **Ortega, R.; Perez, J. A. L.; Nicklasson, P. J.; Sira-Ramirez, H. J.;** 2013. Passivity-based control of Euler-Lagrange systems: mechanical, electrical and electromechanical applications, Springer Science & Business Media, London.
18. **Kim, W.; Won, D.; Shin, D.; Chung, C. C.** 2012. Output feedback nonlinear control for electro-hydraulic systems, Mechatronics 22(6): 766-777.
https://doi.org/ 10.1016/j.mechatronics.2012.03.008.
19. **Alleyne, A. G.; Liu, R.** 2000. Systematic control of a class of nonlinear systems with application to electrohydraulic cylinder pressure control, IEEE transactions on control systems technology 8(4): 623-634.
https://doi.org/ 10.1109/87.852908.
20. **Mazenc, F.; Richard, E.** 2001. Stabilization of hydraulic systems using a passivity property, Systems & Control Letters 44(2): 111-117.
https://doi.org/ 10.1016/S0167-6911(01)00130-X.
21. **He, Y.; Wang, J.; Hao, R.** 2015. Adaptive robust dead-zone compensation control of electro-hydraulic servo systems with load disturbance rejection, Journal of Systems Science and Complexity 28(2): 341-359.
https://doi.org/10.1007/s11424-014-2243-5.
22. **Du, H.; Wang, Z.; Wang, Y.; Huang, H.** 2019. Adaptive robust control of multi-axle vehicle electro-hydraulic power steering system with uncertain tire steering resistance moment, IEEE Access, 7: 5519-5530.
https://doi.org/ 10.1109/ACCESS.2018.2845904.
23. **Yao, J.; Jiao, Z.; Ma, D.** 2015. A practical nonlinear adaptive control of hydraulic servomechanisms with periodic-like disturbances, IEEE/ASME Transactions on Mechatronics 20(6): 2752-2760.
https://doi.org/ 10.1109/TMECH.2015.2409893.
24. **Mobayen, S.** 2015. An adaptive chattering-free PID sliding mode control based on dynamic sliding manifolds for a class of uncertain nonlinear systems, Nonlinear Dynamics 82(1-2): 53-60.
https://doi.org/ 10.1007/s11071-015-2137-7.
25. **Xinliang, L. U.; Fengpo, D. U.; Qian, J. I. A.** 2019. Sliding mode force control of an electrohydraulic servo system with RBF neural network compensation, Mechanics 25(1): 32-37.
https://doi.org/10.5755/j01.mech.25.1.21279.
26. **Guan, C.; Pan, S.** 2008. Adaptive sliding mode control of electro-hydraulic system with nonlinear unknown parameters, Control Engineering Practice 16(11): 1275-1284.
https://doi.org/ 10.1016/j.conengprac.2008.02.002.
27. **Mobayen, S.** 2015. An adaptive chattering-free PID sliding mode control based on dynamic sliding manifolds for a class of uncertain nonlinear systems, Nonlinear Dynamics 2015: 1-8.
https://doi.org/10.1007/s11071-015-2137-7.
28. **Mingxing, Y.; Zhang, Q.; Xinliang, L. U.** 2019. Adaptive sliding mode control of a nonlinear electro-hydraulic servo system for position tracking, Mechanics 25(4): 283-290.
https://doi.org/10.5755/j01.mech.25.4.22822.
29. **Chalanga, A.; Kamal, S.; Fridman, L. M.; Bandyopadhyay, B.; Moreno, J. A.** 2016. Implementation of super-twisting control: Super-twisting and higher order sliding-mode observer-based approaches, IEEE Transactions on Industrial Electronics 63(6): 3677-3685.
https://doi.org/ 10.1109/TIE.2016.2523913.
30. **Gil, J.; You, S.; Lee, Y.** 2021. Super twisting-based nonlinear gain sliding mode controller for position control of permanent-magnet synchronous motors, IEEE Access 9: 142060-142070.
https://doi.org/10.1109/ACCESS.2021.3121127.

H. Du, C. Jing, B. Yan, C. Liu

PASSIVITY-BASED ADAPTIVE ROBUST SUPER-TWISTING NONLINEAR CONTROL FOR ELECTRO-HYDRAULIC SYSTEM WITH UNCERTAINTIES AND DISTURBANCES

S u m m a r y

In this paper, a passive-based adaptive robust super-twisting nonlinear controller (PBARSNC) is proposed for high accuracy torque tracking control of the novel electro-hydraulic loading system with disturbances and uncertainties. The construction of the stability of this electro-hydraulic control system is given using passivity theory that results in a passivity-based controller (PBC). Considering parameter uncertainties and constant or slowly varying disturbances, adaptive law is adopted in the passivity-based controller. Furthermore, super-twisting second-order sliding mode control is used to reject model uncertainties and matched disturbances. Passivity theory, adaptive method and super-twisting algorithm are synthesized via the recursive design method. The proposed passive-based adaptive robust super-twisting nonlinear control can guarantee the torque tracking performance in the presence of various uncertainties, which is very important for high-accuracy tracking control of hydraulic servo systems. Extensive simulations are carried out to verify the high-accuracy tracking performance of the proposed control strategy.

Keywords: passivity, electro-hydraulic system, super-twisting, sliding mode control, adaptive control.

Received September 29, 2022
Accepted January 27, 2023